Detection of Two Isomeric Binding Configurations in a Protein–Aptamer Complex with a Biological Nanopore

Veerle Van Meervelt,[†] Misha Soskine,[†] and Giovanni Maglia*[,†,‡]

[†]Department of Chemistry, KU Leuven, Leuven, B-3001, Belgium and [‡]Groningen Biomolecular Science and Biotechnology Institute, University of Groningen, Groningen, The Netherlands

ABSTRACT Protein–DNA interactions play critical roles in biological systems, and they often involve complex mechanisms and dynamics that are not easily measured by ensemble experiments. Recently, we showed that folded proteins can be internalized inside ClyA nanopores and studied by ionic current recordings at the single-molecule level. Here, we use ClyA nanopores to sample the interaction between the G-quadruplex fold of the thrombin binding aptamer (TBA) and human thrombin (HT). Surprisingly, the internalization of the HT:TBA complex inside the nanopore induced two types of current blockades with distinguished residual current and lifetime. Using single nucleobase substitutions to TBA we showed that these two types of blockades originate from TBA binding to thrombin with two isomeric orientations. Voltage dependencies and the use of ClyA nanopores with two different diameters allowed assessing the effect of the applied potential and confinement and revealed that the two binding configurations of TBA to HT display different lifetimes. These results show that the ClyA nanopores can be used to probe conformational heterogeneity in protein:DNA interactions.

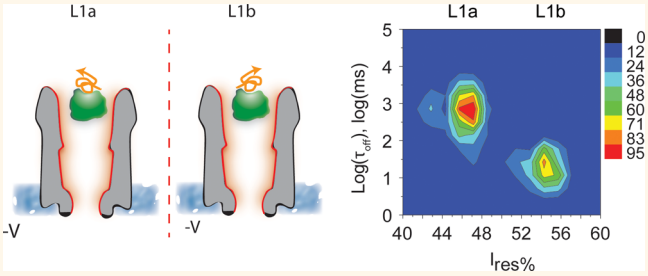

KEYWORDS: single-molecule · nanopore · protein:DNA interactions · thrombin · aptamer

Nanopores have been used to study native proteins at the single-molecule level. The basic principle of nanopore analysis is to observe the disruption of ionic current passing through the nanopore as a molecule occupies the lumen of the pore. Much of the initial attention has focused on using proteins to control the translocation of DNA across nanopores for DNA sequencing applications.[1,2] Unfolded proteins have been recently studied by observing the ionic current blockades provoked by their translocation through biological nanopores.[3−12] Folded proteins, which are too large to pass through the biological nanopores commonly used, have been studied by recording their translocation through artificial nanopores, either alone[13−20] or in complex with DNA.[21−24] However, protein translocation through solid-state nanopores is usually too rapid[25] to observe the kinetic and thermodynamic properties of the protein:DNA complex. We recently showed that proteins can be studied using the cytolysin A (ClyA) biological nanopore from *Salmonella typhi* (ClyA-CS).[26−28] Conveniently, we found that two types of ClyA nanopores can be isolated, which we named type I and type II ClyA. The two nanopore types run differently on Blue Native PAGE and displayed distinguished current signatures when blocked by protein analytes. Comparison of their open pore currents with theoretical conductance values suggested that type I and type II ClyA might correspond to the 12-mer and 13-mer oligomeric forms of ClyA observed by X-ray and Cryo-EM experiments, respectively.[26]

The internal surface of ClyA is negatively charged;[29] thus under negative applied potentials (*trans*) there is a vectorial flux of water and cations through the nanopore, the electroosmotic flow (EOF), from *cis* to *trans*. In ClyA[17,27] and other nanopores,[17] the EOF promotes the entry of proteins inside the nanopore irrespectively of the protein charge. Remarkably, we found that at certain applied potentials (*e.g.*, >−35 mV) the ClyA nanopore acts as a nanotrap where the Brownian motion of proteins is

* Address correspondence to giovanni.maglia@chem.kuleuven.be, g.maglia@rug.nl.

Received for review October 24, 2014 and accepted December 10, 2014.

Published online December 10, 2014
10.1021/nn506077e

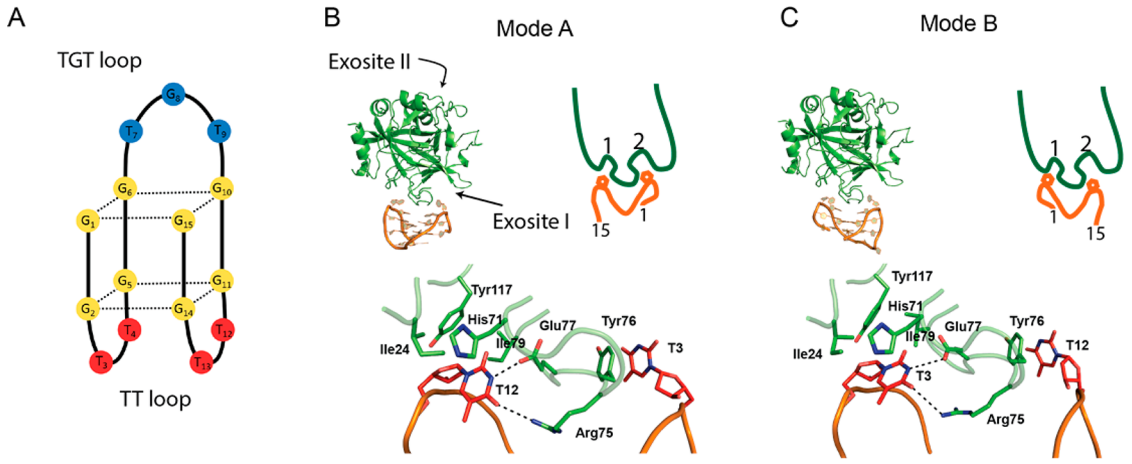

Figure 1. Binding of TBA to HT. (A) Schematic representation of TBA. The central G-tetrad core is shown in yellow, the TGT loop in blue, and the TT loops in red. (B) HT:TBA mode A as observed in a first crystallographic study (PDB_ID 1HAO)[43] where T12 forms a hydrogen bond interaction with Glu77 and Arg75 and sits in a hydrophobic pocket formed by Ile24, His71, Ile79, and Tyr117. T3 forms a π-stacking interaction with Tyr76. (C) HT:TBA mode B as described in a subsequent crystal structure (PDB_ID 4DIH),[44] where T3 forms the hydrogen bond-mediated interactions with Glu77 and Arg75 and hydrophobic interactions with Ile24, His71, Ile79, and Tyr117. T12 forms a π-stacking interaction with Tyr76. HT, in green, and the aptamer, in orange, are in cartoon representation (Pymol). At the bottom end of panels B and C T3 and T12 in TBA and His71, Arg75, Glu77, Ile79, and Tyr117 in HT are in stick representation. The right corner of panels B and C shows the graphic representation of the HT:TBA interaction with HT and TBA.

balanced by the EOF, and proteins such as human thrombin (HT) are confined inside the nanopore lumen for up to tens of minutes.[26,27] Above a threshold potential (*e.g.*, ~90 mV for type I ClyA-CS nanopores) the mean dwell time of HT blockades decreased with increasing the applied potential,[26] suggesting that the additional drag force produced by the increased electroosmotic flow promotes the translocation of the protein through the pore.[26]

The aim of this work is to assess the ability of the ClyA biological nanopores to investigate protein:DNA interactions. The recognition and binding of specific sites on DNA by proteins is central for many cellular functions such as transcription, replication, and recombination. Recently, it appeared clear that genomic DNA can adopt sophisticated three-dimensional structures that are able to interact with proteins. For example, G-rich sequences can form various G-quadruplex structures in genomic DNA[30] that have been shown to be important for chromosomial maintenance in eukaryote telomers[31] or to control gene expression of various genes.[32,33] Several ensemble studies have addressed the interaction between proteins and DNA-based[34] or RNA-based[35] G-quadruplexes. The interactions between proteins and their DNA partners often involve complex mechanisms and might be spatially and temporally inhomogeneous. Studies have shown that the binding geometry of the same protein can vary when bound to a different[36−38] or even to the same DNA sequence.[39] For example, it was shown that one of the activator proteins, AP-1, binds to DNA with two distinct orientational isomers related by a 180° rotation,[40] with each conformation having different transcriptional potency.[41] Binding heterogeneity and unsynchronized biochemical events, however, are not easily studied by ensemble techniques.

As a model system to sample protein:DNA interactions, we investigated the binding between HT and a thrombin binding aptamer (TBA).[42] TBA folds in an antiparallel G-quadruplex structure where the G-tetrad central core of the aptamer is connected by two TT loops at one side and a TGT loop at the other side (Figure 1A). The binding of HT to TBA has been intensively studied. Initial X-ray reports showed that the TT loops in TBA bind to the exosite I in thrombin in a pincer-like fashion (Figure 1B,C). Interestingly, however, the TT loops of TBA were crystallized with HT in two isomeric configurations, in which the aptamers are oriented 180° around their quadruplex axis. In mode A [PDB_ID:1HAO[43]] T12 of TBA is in hydrogen bond contact with Glu77 and Arg75 and sits in a hydrophobic pocket formed by Ile24, His71, Ile79 and Tyr117 in HT. T3 in the opposite site of the loop forms a π-stacking interaction with Tyr76 (Figure 1B). In mode B [PDB_IDs: 4DII or 4DIH[44]] T3 and T12 in TBA form the same set of interactions with HT but in reverse order (Figure 1C). Notably, substituting the T3 and T12 nucleobases in the TT loops with abasic nucleotides (TBA-ΔT3 and TBA-ΔT12, respectively) produced two crystal structures in which the aptamer was binding to HT in either mode A (TBA-ΔT3, PDB_ID:4LZ4) or mode B [TBA-ΔT12, PDB_ID: 4LZ1[45]], strongly suggesting that in solution TBA might bind to thrombin with either of two isomeric configurations.

Several previous studies described the interaction of aptamers or G-quadruplex DNA folds with biological nanopores,[22,46−50] and the interaction between HT and TBA has been monitored using nanopores decorated

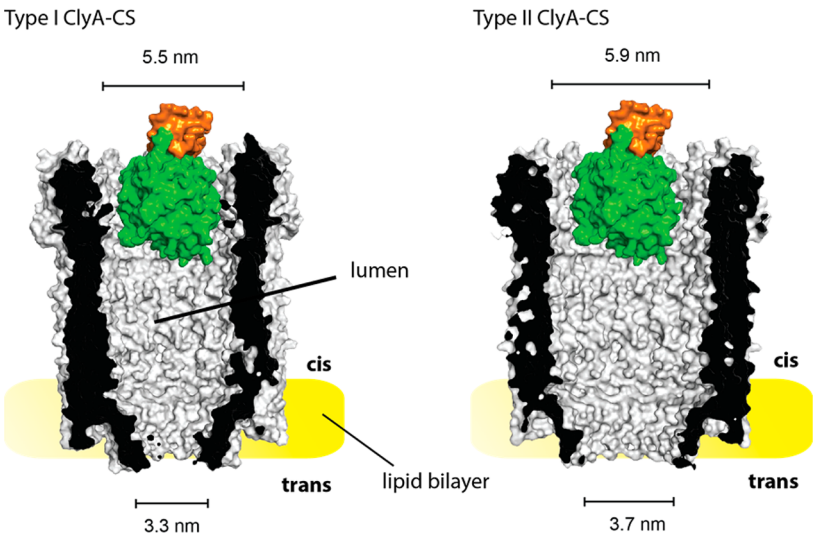

Figure 2. Surface representation of the putative residence of HT:TBA inside type I ClyA-CS (left) and type II ClyA-CS (right) nanopores. Cut-through structures were generated with Pymol. The structure of the HT:TBA complex is taken from ref 43 (PDB_ID: 1HAO). The values of the *cis* and *trans* diameters include the van der Waals radii of the atoms.

with aptamers.[27,51] However, since the aptamers were attached to the nanopore mouth, details of the aptamer: protein interaction could not be revealed. Here we describe a new approach in which the protein:DNA aptamer complex is trapped inside the ClyA nanopore. We show that at −140 mV the electroosmotic flow acting on the protein:DNA complex is counterbalanced by a combination of steric hindrance, electrophoretic forces that act on the DNA, and electrostatic interactions between the DNA and the nanopore (Figure 2). When the complex is dissociated, the aptamer is ejected from the pore and HT is internalized deeper inside the nanopore, as shown by the switching of the ionic signal to a lower residual current level typically observed when free HT molecules enter the ClyA nanopore. Remarkably, the trapped protein:DNA complex induced two ionic current blockades showing different mean dwell time and residual current values, which corresponded to the two isomeric binding configurations of HT:TBA recently identified by structural studies.[44,45] These results indicate that the ClyA nanopore acts as a nanotrap in which isomeric configurations of protein:DNA interactions can be studied.

RESULTS

Interaction of HT with ClyA Nanopores. The interaction of thrombin with TBA aptamers was sampled using type I and type II ClyA-CS nanopores. ClyA-CS (L99Q, E103G, F166Y, C285S, K294R) is a version of *S. typhi* ClyA that was selected from random mutagenesis libraries for its favorable characteristics for nanopore experiments, which includes highly water-soluble monomers, low bandwidth noise, and lack of gating behavior in planar lipid bilayers. The nanopores were reconstituted from the *cis* chamber and the potential applied to the *trans* compartment. The orientation of the pore could be assessed by the slightly asymmetric current−voltage relationship of the nanopores.[27] At −140 mV and in 15 mM Tris-HCl, 140 mM NaCl, and 5 mM KCl, pH 7.5, type II ClyA-CS nanopores displayed a conductance of 1.64 ± 0.05 nS (mean ± SD, N = 42 single-channel experiments) and type I ClyA-CS nanopore showed a conductance of 1.38 ± 0.03 nS (N = 10). At −140 mV, the addition of 10 nM HT in the *cis* compartment produced blockades (I_B) to the open pore conductance (I_O) quoted here as residual current percent ($I_{res\%} = I_B/I_O \times 100$), due to the entry of HT into the nanopore vestibule.[26] Thrombin blockades to type I ClyA-CS and type II ClyA-CS showed a blocked pore current level L2-HT of 19.2 ± 0.8% (N = 9) and 25.9 ± 2.0% (N = 26), respectively. Previous studies suggested that L2-HT most likely described HT lodging deep inside the nanopore lumen.[26,28] L2-HT blockades to type I and type II ClyA-CS showed a lifetime (τ_{off}) of 612 ± 112 ms (N = 9, n = 1316 events) and 1.4 ± 0.6 ms (N = 9, n = 2152), respectively, and appeared with a frequency (f) of 0.26 ± 0.05 s^{-1} nM^{-1} and 0.26 ± 0.16 s^{-1} nM^{-1} (N = 9 and N = 22), respectively.

Measuring the Affinity Binding Constant for the HT:TBA Complex. The addition of the DNA aptamer TBA [d(GGTTGGTGTGGTTGG] to the *cis* solution of type I ClyA-CS or type II ClyA-CS nanopores reduced the frequency of HT current blockades and induced a new type of current blockades due to the capture of the HT:TBA complex inside the nanopore cavity (Figure 3A). By contrast, the addition of 400 nM of DNA with a random sequence produced no visible effect on the HT-induced current blockades (not shown). The equilibrium dissociation constant K_d for the binding of HT to TBA was measured by titration experiments using type I and II ClyA-CS nanopores. Increasing the concentration of TBA decreased the capture frequency of

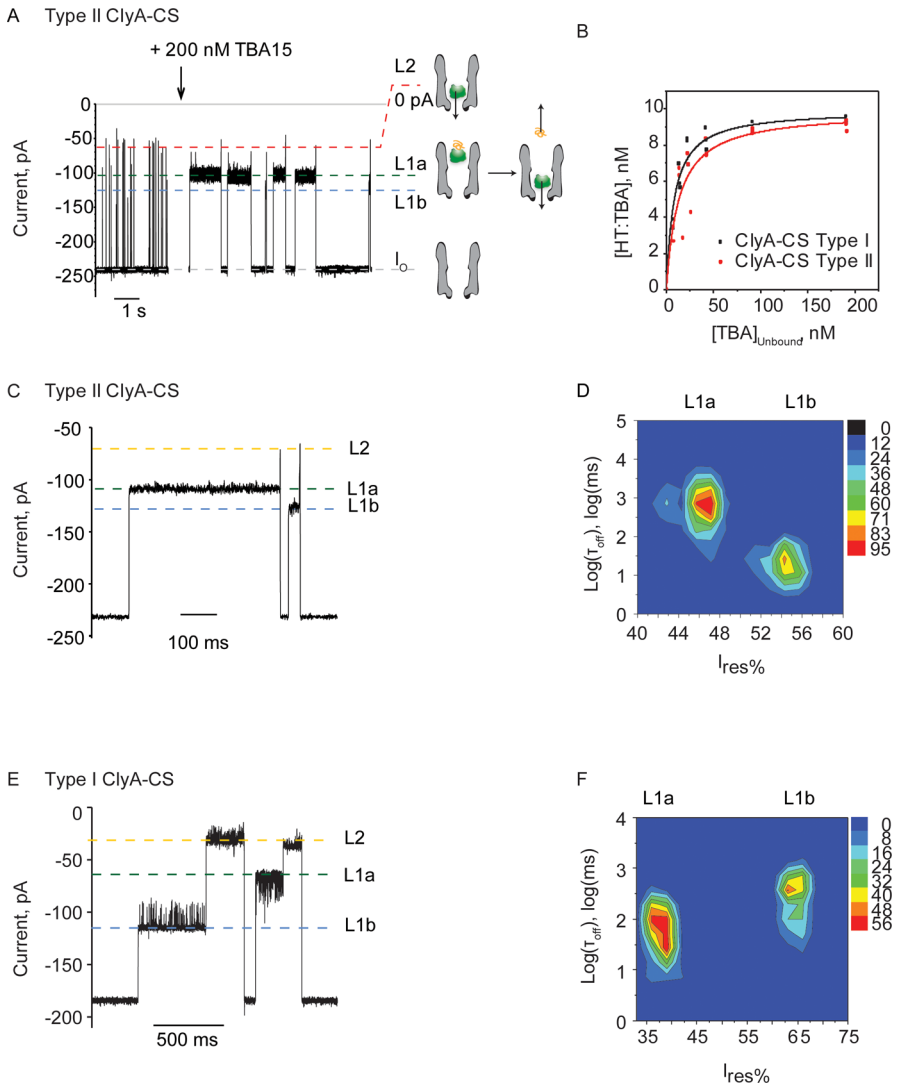

Figure 3. Capture of the thrombin:TBA complex. (A) Typical blockades to type II ClyA-CS showing the capture of HT (10 nM, added to the *cis* solution) and the blockades induced by the HT:TBA complex (right) after the addition of 200 nM TBA to the *cis* solution. L2 blockades are due to the internalization of HT; L1a and L1b blockades to the capture of the HT:TBA complex. A likely interpretation of the current blockades is shown by the cartoon representation on the right of the current trace. (B) Determination of the dissociation constant for the HT:TBA complexes by titration experiments using ClyA-CS type I (black squares) or ClyA-CS type II nanopores (red circles). The concentration of unbound TBA and of the HT:TBA complex was calculated as described in the Materials and Methods. (C) Selected L1a and L1b current blockades to type II ClyA-CS nanopores. (D) Contour plot of L1a and L1b blockades to type II ClyA-CS nanopores. (E) Two consecutive L1a and L1b current blockades to type I ClyA-CS nanopores. (F) Contour plot of L1a and L1b blockades to type I ClyA-CS nanopores. Experiments were performed at −140 mV in 15 mM Tris-HCl, 140 mM NaCl, and 5 mM KCl, pH 7.5. Data were recorded by applying a 2 kHz low-pass Bessel filter with 10 kHz sampling rate. An additional postacquisition digital Gaussian filter at 2 kHz was applied to the current traces.

unbound HT by the nanopore, reflecting the decreasing concentration of unbound HT in solution. Fitting to a one-site binding isotherm gave the apparent K_d value of 8 ± 1 nM (N = 3 experiments) and 13 ± 3 nM (N = 3) for type I and type II ClyA-CS, respectively (Figure 3B).

HT:TBA Complex Produces Two Current Blockades. Most of the HT:TBA blockades showed an initial current level (L1) that often switched to a L2-HT current level. A likely physical interpretation of the current blockades, given in Figure 3A, is that the negatively charged aptamer prevents the full internalization of the complex inside the nanopore. After the HT:TBA complex is disassembled, HT is internalized deeper inside the nanopore and then the protein is released from the pore. TBA is most likely ejected back into the *cis* solution, as DNA does not translocate through ClyA under these conditions.[28] Interestingly, two distinct L1 ionic current blockades, named here L1a and L1b, were observed for the interaction of HT:TBA with the ClyA-CS nanopores (Figure 3C–F). Using type II ClyA-CS, 62 ± 4% (N = 6 experiments) of the current blockades appeared with a L1a HT:TBA level ($I_{res\%}$ = 45.7 ± 0.9%, N = 6, and τ_{off} = 1.02 ± 0.18 s, N = 4, n = 972 events), and the remaining blockades appeared with an L1b level ($I_{res\%}$ = 53.6 ± 0.9%, N = 6, and τ_{off} = 25 ± 2 ms, N = 4, n = 710). The percentage of L1a and L1b blocks did not depend on

TABLE 1. Parameters for the HT:Aptamer Blockades to Type I ClyA-CS and Type II ClyA-CS Nanopores[a]

	$I_{res\%}$	τ_{off} (ms)	ΔU (kcal mol^{-1} V^{-1})	$k_{off,0\ mV}$ (s^{-1})	K_d (nM)
			Type II ClyA-CS		
TBA (L1a)	45.7 ± 0.9	1019 ± 179	15.5 ± 3.7	2.57 ± 2.10 × 10^{-2}	13 ± 3
TBA (L1b)	53.6 ± 0.9	25 ± 2	8.5 ± 1.0	5.31 ± 1.16	
TBA-T3A (L1a)	45.6 ± 0.5	3301 ± 1717	17.2 ± 6.1	5.83 ± 7.80 × 10^{-3}	6 ± 1
TBA-T12A (L1b)	53.8 ± 0.3	52 ± 5	11.0 ± 1.9	1.46 ± 0.62	7 ± 1
TBA-ΔT3 (L1a)	46.0 ± 1.3	348 ± 57	14.2 ± 1.9	9.26 ± 3.89 × 10^{-2}	22 ± 4
TBA-ΔT12 (L1b)	54.5 ± 1.1	9 ± 1	6.9 ± 0.2	21.51 ± 1.07	54 ± 29
			Type I ClyA-CS		
TBA (L1a)	35.6 ± 0.7	118 ± 15	10.0 ± 1.7	0.90 ± 0.34	8 ± 1
TBA (L1b)	62.0 ± 0.8	386 ± 18	2.5 ± 0.2	1.40 ± 0.07	

[a] $I_{res\%}$ is the residual current, τ_{off} the lifetime, $k_{off,0\ mV}$ the extrapolated dissociation rate at 0 mV, ΔU the reduction in the HT:TBA dissociation energy barrier due to the applied potential V, and K_d the complex dissociation affinity constant. Errors are stated as standard deviations.

the applied potential (from −100 to −150 mV) or the concentration of TBA used. In 87 ± 2% of the events, the L1 (HT:TBA) blockades terminated with a transient L2-HT current blockade ($I_{res\%}$ = 25.8 ± 1.7%, N = 6, and τ_{off} = 0.7 ± 0.3 ms, N = 6, Figure 3A,C and Figure S1). The analysis of HT:TBA current blockades to type I ClyA-CS nanopores revealed a similar pattern of interactions (Figure 3 E,F and Figure S2). L1a and L1b blockades showed an $I_{res\%}$ value of 35.6 ± 0.7% and 62.0 ± 0.8% (N = 7), respectively, and a mean dwell time value of 118 ± 15 ms (N = 7, n = 1724) and 386 ± 18 ms (N = 7, n = 1493), respectively. Finally, L1a blockades were 54 ± 3% (N = 7) of the total (Table 1).

Single Base Substitutions to the TT Loop Induced One Type of HT:TBA Current Blockades. To investigate the nature of the TBA-induced current blockades, we tested four single base substitutions to the aptamer using the type II ClyA-CS nanopores. Guided by crystallographic evidence (Figure 1), we targeted the TT loop at position 3 or 12, aiming to disrupt the symmetry in HT binding. Remarkably, substitution of T3 with an abasic residue (TBA-ΔT3) produced only L1a blockades ($I_{res\%}$ = 46.0 ± 1.3%, N = 6 experiments) that showed a ∼3-fold reduced lifetime with respect to the L1a blockades of TBA (τ_{off} = 348 ± 57 ms, N = 3, n = 1241 events, Table 1, Figure 4). The substitution of T3 with adenine (TBA-T3A) also produced only L1a current blockades ($I_{res\%}$ = 45.6 ± 0.5%, N = 6 and τ_{off} = 3.3 ± 1.7 s, N = 3, n = 490), but with a ∼3-fold increased lifetime compared to TBA blockades. Notably, the equivalent substitutions at position 12 (TBA-T12A and TBA-ΔT12) produced only L1b blockades. Similarly to what was observed with L1a blockades, TBA-T12A blockades showed an ∼2-fold increased lifetime (τ_{off} = 52 ± 5 ms, N = 3, n = 1743) and TBA-ΔT12 a ∼3-fold reduced lifetime (τ_{off} = 9 ± 1 ms, N = 3, n = 1042) with respect to the values measured for TBA (Table 1, Figure 4). These results suggest, therefore, that the L1a and L1b blockades might be related to the binding of TBA to HT in the two binding modes previously described in different X-ray structures.

Determination of the Aptamer Dissociation Rate Constants. The dissociation rate constant k_{off}, calculated from the inverse of τ_{off}, increased with the applied potential, most likely reflecting the effect of the applied potential on the DNA charge (Figure 5). Using the van't Hoff Arrhenius formalism, the dissociation rate might be described by $k_{off} = k_{off,0\ mV} \exp(|V|\Delta U/RT)$, where $k_{off,0\ mV}$ is the zero voltage dissociation rate constant, R the gas constant, T the temperature, and ΔU the reduction in the energy barrier due to the applied potential V. It follows that

$$\ln(k_{off}) = \ln(k_{off,0mV})(|V|\Delta U/RT) \quad (1)$$

Fitting eq 1 to the data in Figure 5 revealed that the effect of the applied potential was different for L1a and L1b blockades and among nanopores with different size (Table 1). L1a blockades showed stronger voltage dependence than L1b blockades in both nanopores, while type I ClyA-CS nanopores produced blockades that were less influenced by the applied potential than type II ClyA-CS nanopores (Table 1). Further, L1a blockades to type II ClyA-CS nanopores showed a dissociation rate constant at zero applied potential that was about 2 orders of magnitude smaller than the $k_{off,0\ mV}$ values for L1b blockades (Table 1). By contrast, the L1a and L1b blockades to type I ClyA-CS nanopores showed similar values.

DISCUSSION

TBA Binds to HT with Two Isomeric Configurations. In this work we showed that the interaction of the G-quadruplex structure of TBA with HT can be studied using type I and type II ClyA-CS nanopores. K_d values for the aptamer:thrombin interaction, calculated by measuring the frequency decrease of HT blockades as a function of TBA (Figure 3B), were compatible with previously reported K_d values measured with other methods (20−450 nM).[42,52−56] Surprisingly, however, we found that the blockades produced by HT:TBA showed two distinctive current signals, L1a and L1b. Previous X-ray crystallography data suggested that

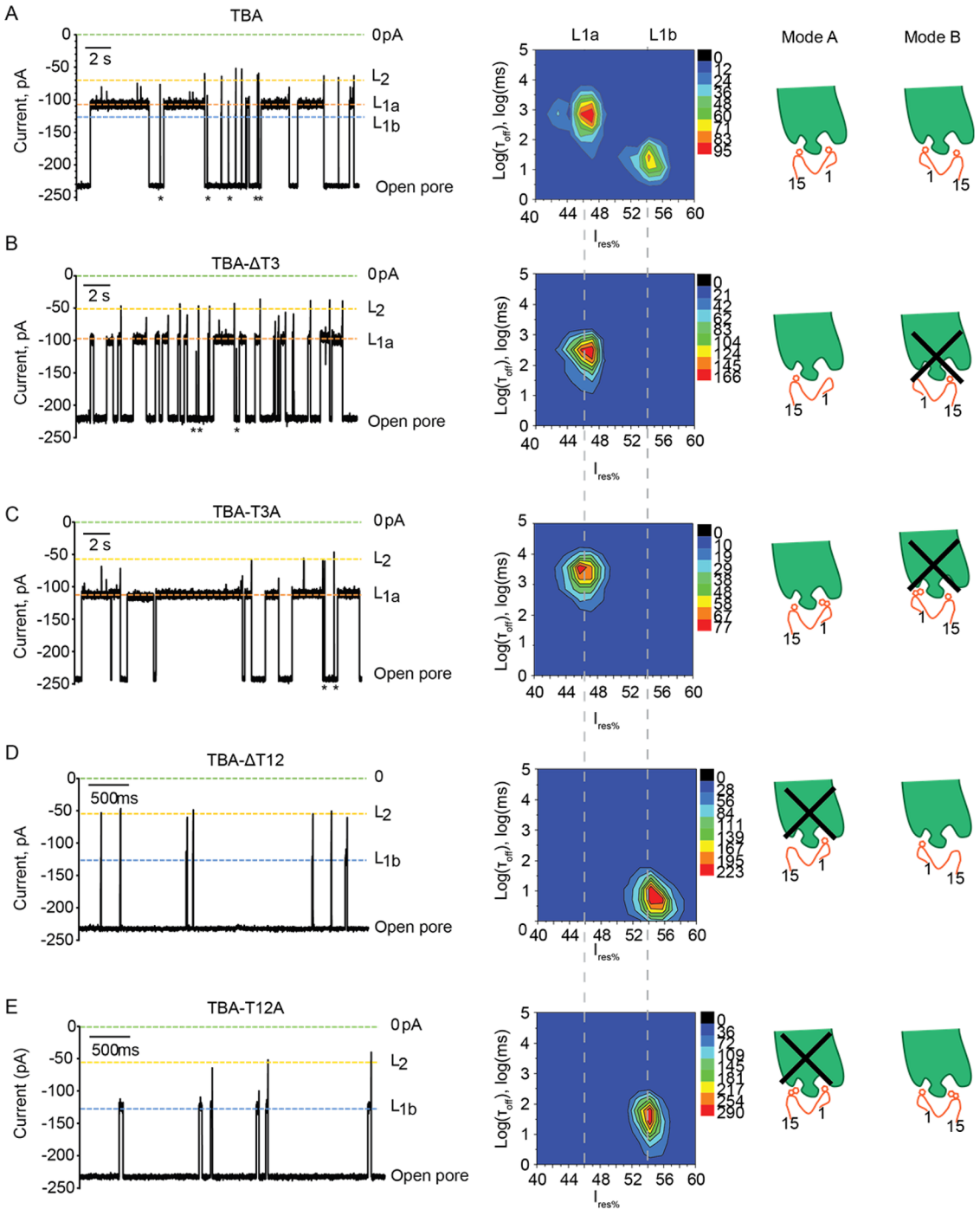

Figure 4. Binding of DNA aptamers to HT. (A) Binding of TBA to HT gives two different current blockades to type II ClyA-CS, representing the two modes of binding of the aptamer to HT. The capture of unbound HT is indicated with an asterisk. TBA-ΔT3 (B) or TBA-T3A (C) in complex with HT produces only L1a blockades to type II ClyA-CS, corresponding to the binding of TBA to HT in mode A. TBA-ΔT12 (D) or TBA-T12A (E) in complex with HT produces only L1b blockades to type II ClyA-CS, corresponding to binding in mode B. Experiments were performed at −140 mV in 15 mM Tris-HCl, 140 mM NaCl, and 5 mM KCl, pH 7.5. Data were recorded by applying a 2 kHz low-pass Bessel filter with 10 kHz sampling rate. An additional postacquisition digital Gaussian filter at 2 kHz was applied to the current traces.

TBA might interact with HT in two distinctive configurations. In an early structure (PDB_ID: 1HAO[43]) T12 in the TT loop of TBA was in hydrogen bond contact with Glu77 and Arg75, while T3 in the opposite site of the loop formed a π-stacking interaction with Tyr76. We name this interaction mode A (Figure 1). In subsequent structures (PDB_ID: 4DII or 4DIH[44]) TBA showed the same interactions, although T3 and T12 switched in position. This interaction was named mode B (Figure 1). Recent X-ray crystallography data confirmed that TBA most likely binds in two conformations. The substitution of T3 in TBA with an abasic nucleobase (TBA-ΔT3)

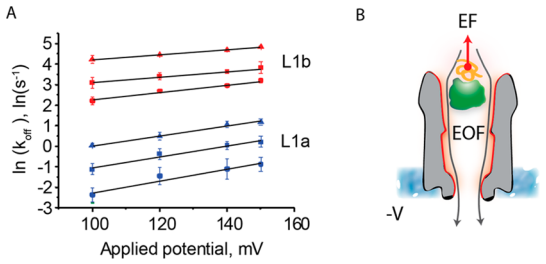

Figure 5. Measurement of aptamer:protein binding constants. (A) Voltage dependency of the dissociation rate constants (k_{off}) for the aptamers binding to HT measured with type II ClyA-CS. L1a blockades are shown in blue and L1b blockades in red. The blockades induced by TBA are shown as red and blue squares, TBA-ΔT3 are in blue triangles, TBA-ΔT12 are in red triangles, TBA-T3A are in blue spheres, and TBA-T12A are in red spheres. (B) Forces acting on the HT:DNA complex. Electrophoresis (EF) is likely to oppose the internalization of the HT:TBA complex, while the electroosmotic flow (EOF) promotes the capture of the complex. The electrostatic repulsion between the DNA aptamer and the negative charges lining the internal surface of the nanopore, shown as a red line, is also likely to play a role by opposing the confinement and promoting the dissociation of the HT:TBA complex.

produced a complex in mode A (PDB_ID: 4LZ4), while the equivalent nucleobase substitution at position 12 (TBA-ΔT12) produced a structure with the complex in mode B (PDB_ID: 4LZ1[45]).

In order to test whether L1a and L1b current blockades were due to the HT:TBA complex entering the ClyA nanopore in mode A or B, we tested nucleobase substitutions to TBA at position 3 or 12. The substitution of T3 with adenine (TBA-T3A) or with an abasic nucleotide (TBA-ΔT3) induced HT:TBA blockades that showed only L1a levels. The equivalent substitution at position 12 (TBA-T12A and TBA-ΔT12) induced blockades that showed only L2b levels (Figure 4). These results strongly suggest that the two isomeric HT:TBA conformers induce different ionic current blockades once internalized inside the lumen of ClyA nanopores, with L1a blockades corresponding to HT:TBA entering the ClyA-CS nanopore in mode A and L1b blockades corresponding to HT:TBA entering the nanopore in mode B. The relative concentration of HT:TBA in mode A and mode B could be estimated from the capture frequency measured with TBA-T3A and TBA-T12A, respectively, using type II ClyA-CS nanopores (Figure S3). We found that the species corresponding to the L1a blockades were 2.0 ± 0.8-fold more abundant than the species corresponding to the L1b blockades, suggesting therefore that the TBA binds to HT with slightly higher affinity in mode A than in mode B.

Electroosmotic and Electrophoretic Effects on the Complex Internalization. As previously shown,[17,27] proteins enter the ClyA lumen following the electroosmotic flow, which arises from the flow of water that is driven by directional movement of cations through the cation-selective ClyA nanopore. A molecule with a net charge density Q inside a nanopore also experiences an electrophoretic force, EF = $V_{bias}Q$, due to the electric field in the nanopore. At negative applied potentials (*trans*) the EF opposes the internalization of DNA molecules added to the *cis* chamber. Therefore, the EOF, which for ClyA under negative applied potentials is from *cis* to *trans*, is the most likely force that promotes the capture and confinement of the protein:DNA complex inside the nanopore. Other factors that oppose the entry of DNA into ClyA are steric hindrance and electrostatic repulsion from the negatively charged ClyA lumen. We found that the lifetime of the L1a and L1b HT:TBA complexes decreased with increasing applied potential. Therefore, the EF on the bare charge of DNA, steric hindrance, and electrostatic effects oppose the complex translocation, on one hand, and promote the dissociation of the complex on the other hand (Figure 5B).

Effect of Nanopore Confinement on the HT:TBA Binding Constants. The extrapolated value of the dissociation rate constant at zero applied potential ($k_{off,\ 0\ mV}$) for L1a blockades to type II ClyA-CS nanopores was 2.57×10^{-2} s^{-1}, a value similar to the dissociation rate constant for the thrombin:aptamer interaction determined previously by nanopores with covalently attached aptamers,[51] by surface plasmon resonance (SPR),[57,58] or by capillary electrophoresis studies[54−56] (1×10^{-1} to 4×10^{-3} s^{-1}). The wide range of values most likely reflects the limitations associated with the techniques used, that is, the use of high ionic strength (1 M KCl) in the nanopore experiments, the effect of surface immobilization in SPR experiments, or the effect of the applied potential in capillary electrophoresis experiments. Our approach is also likely to suffer from limitations related to the confinement of the complex inside the nanopore and the electrostatic interactions between the HT:TBA complex and the lumen of the nanopore. In fact, using type I ClyA-CS nanopores, the $k_{off,\ 0\ mV}$ values for L1a and L1b blockades were 1 order of magnitude higher than the L1a values measured with larger type II ClyA-CS nanopores (Table 1). Further, we also found that the mean dwell times for L1a blockades to type II ClyA-CS nanopores were remarkably longer than for L1b blockades (Table 1). This is surprising, because HT and TBA in the two binding configurations have the same set of interactions and have similar binding affinities (see above), as indeed observed for the τ_{off} values for L1a and 1b blockades to type I ClyA-CS nanopores.

Although the confinement of the protein:DNA complex inside ClyA-CS is likely to influence the dissociation of the HT:TBA complex, some thermodynamic parameters might still be retrieved, for example by comparing the mean dwell times of individual blockades obtained from aptamers with single base substitutions. Abasic substitutions at position 3 in TBA reduced ~3-fold the mean dwell time of L1a blockades, while the substitution of T3 with adenine increased the mean

dwell time of L1a blockades by about 3-fold (Table 1). The same substitutions at position 12 in TBA produced a similar effect on the mean dwell time of L1b blockades, despite the remarkable difference shown by the mean dwell time values of L1a and L1b blockades (Table 1). Therefore, using the Eyring−Polanyi equation it is possible to calculate the contribution of the π-stacking interaction between the DNA aptamer and HT, an interaction commonly found in DNA binding proteins.[59] From the average values of the dissociation rates measured from L1a and L1b blockades (Table 1), we found that thymine stabilized the HT:TBA interaction by 0.6 kcal mol^{-1} and adenine by 1.2 kcal mol^{-1}.

CONCLUSION

We have shown that ClyA biological nanopores can sample the interaction between thrombin and the G-quadruplex fold of the thrombin binding aptamer. The binding affinity constant for the aptamer:protein interaction is easily measured by following the reduction of the frequency of the HT blockades provoked by the binding of the aptamer. One additional advantage of this technique is that at high negative applied potentials the protein:DNA complex can be trapped inside the nanopore and analyzed by electrical recordings. The captured HT:TBA complex provoked two kind of blockades that were clearly distinguished by their residual current and lifetime values. Modifications to the TBA sequence allowed the assignment of the two current blockades to two isomeric binding configurations, mode A and B (Figure 1), recently observed in two crystallographic studies, in which the TBA rotated by 180° around the TBA G-quadruplex axis. Nanopore recordings revealed that the HT in mode A has a higher binding affinity for TBA than its isomeric binding configuration. Therefore, the ClyA nanopore provides a new tool that might be useful for the identification of subtle heterogeneity in protein:DNA complexes.

MATERIALS AND METHODS

All materials were purchased from Sigma-Aldrich, enzymes were from Fermentas, and DNA was from Integrated DNA Technologies (IDT) unless otherwise specified. Throughout the text, *N* indicates the number of independent experiments and *n* the total number of data points in the data set.

Preparation of Aptamers and Human Thrombin. The sequences of the aptamers are listed in Table 2. Stock solutions of DNA aptamers were prepared by dissolving the lyophilized powder in 10 mM Tris-HCl, pH 8.5, up to a concentration of 100 μM. Aliquots were then stored at −20 °C. Stock solutions of human thrombin were prepared by dissolving the lyophilized protein (Sigma-Aldrich) in H_2O up to a concentration of 0.2 NIH units/μL and were aliquoted and stored at −20 °C. The molar concentration of HT was calculated from its unit concentrations, with 1 NIH unit/mL = 10 nM.[60]

Expression and Purification of ClyA Nanopores. In this work we used an engineered variant of ClyA from *Salmonella typhi*, ClyA-CS, which contains L99Q, E103G, F166Y, C285S, and K294R mutations relative to ClyA-WT and a C-terminal hexahistidine tag. ClyA-CS monomers were expressed in E. cloni EXPRESS BL21 (DE3) cells and purified using Ni-NTA affinity chromatography. Oligomers were then formed by adding 0.2% *n*-dodecyl-beta-D-maltoside (DDM, GLYCON Biochemicals GmbH). Type I ClyA-CS and type II ClyA-CS oligomers were separated from monomers and several other oligomeric ClyA forms[27] using a blue native polyacrylamide gel electrophoresis (BN-PAGE, Bio-Rad). In this work we gel extracted the lowest and the second lowest band, which are likely to correspond to the 12-meric (ClyA type I) and 13-meric (ClyA type II) form of ClyA. Aliquots were stored at 4 °C in 0.2% DDM and 10 mM EDTA.[27]

Electrical Recordings in Planar Lipid Bilayers. Single-channel recordings were performed as described before.[61] In short, a 1,2-diphytanoyl-*sn*-glycero-3-phosphocholine (Avanti Polar Lipids) lipid bilayer was formed across a ~100 μm Teflon (Goodfellow Cambridge Limited) aperture separating two compartments (*cis* and *trans*) filled with 140 mM NaCl, 5 mM KCl, and 15 mM Tris-HCl, pH 7.5. An electrical potential was applied to the *trans* side using Ag/AgCl electrodes. ClyA nanopores were inserted into lipid bilayers from the *cis* compartment, which was connected to the ground. After the insertion of a single nanopore, the excess of protein was removed by several cycles of perfusion. Human thrombin was added to the *cis* chamber at a final concentration of 10 nM. Aptamer solutions (Table 2) were added at concentrations ranging from 10 to 500 nM and were incubated with thrombin in the electrophysiology chamber for 5 min prior to recording.

Data were recorded by applying a 2 kHz low-pass Bessel filter and using a 10 kHz sampling rate. An additional digital Gaussian filter at 2 kHz was applied postacquisition to the current recordings. The electrical signals were amplified by using an Axopatch 200B patch clamp amplifier (Axon Instruments) and digitized with a Digidata 1320 A/D converter (Axon Instruments). Data were recorded by using Clampex 10.2 software (Molecular Devices), and the subsequent analysis was carried out with Clampfit software (Molecular Devices) and OriginPro 8.6 (OriginLab). All experiments were carried out at 24 °C.

Determination of the Thrombin:Aptamer Complex Blockades. Residual current values ($I_{res\%}$) were calculated from blocked pore current values (I_B) and open pore current values (I_O) as $I_{res\%} = 100 \times I_B/I_O$. I_B was determined from Gaussian fits to all HT:aptamer events collected using the "single-channel search" function in Clampfit. I_O was determined from the Gaussian fit to all point current histograms.

The dissociation constant (K_d) of the HT:aptamer complex was determined from titration experiments. The HT concentration was 10 nM, and aptamers were added from a stock solution (10 or 100 μM). The concentration of HT:TBA complexes was measured from the frequency of unbound thrombin capture at −140 mV as $[HT:TBA] = 10 - [HT]_{unbound}$. The concentration of unbound aptamer $[TBA]_{unbound}$ was calculated from the initial concentration of TBA ($[TBA]_0$) as $[TBA]_{unbound} = [TBA]_0 - (10 - [HT]_{unbound})$, where $[HT]_{unbound}$ was measured from the frequency of unbound thrombin capture at −140 mV. The plot of the concentration of HT:TBA blockades *versus* the concentrations of $HT_{unbound}$ gave a saturation curve that was then fitted according to the one-site binding isotherm. The K_d is the concentration of aptamer at 50% signal saturation.

The lifetimes of the HT:aptamer complexes were determined at 100, 120, 140, and 150 mV by using the "single-channel search" function in Clampfit. A threshold level was set for the complex blockades. Events shorter than 2 ms were ignored in the analysis of TBA, TBA-T3A, TBA-ΔT3, and TBA-T12A experiments. No additional limitations were set for the analysis of TBA-ΔT12 experiments. The process of event collection was monitored manually. The resulting event lifetimes (τ_{off}) from one experiment were binned together as cumulative distributions and fitted to a single exponential to retrieve the lifetimes of the complexes (τ_{off}). Finally, the average of the obtained k_{off} values, calculated as $1/\tau_{off}$, for each experiment was calculated.

TABLE 2. Sequences of the Aptamers Used in This Work

name	sequence[a]
TBA	5′-GGTTGGTGTGGTTGG-3′
TBA-T3A	5′-GG**A**TGGTGTGGTTGG-3′
TBA-T12A	5′-GGTTGGTGTGG**A**TGG-3′
TBA-ΔT3	5′-GG-**dS**-TGGTGTGGTTGG-3′
TBA-ΔT12	5′-GGTTGGTGTGG-**dS**-TGG-3′
random DNA	5′-CACCATCACCACCATCAT-3′

[a] **-dS-** indicates an abasic furan site (1′,2′-dideoxyribose or dSpacer, IDT).

I_{res} *versus* lifetime distribution plots were generated using the Origin86 software (OriginLab).

The capture frequency of HT:TBA complexes was determined at −140 mV using the "single-channel search" function of Clampfit. The concentration of the species corresponding to L1a and L1b events was calculated by assuming that the capture frequency measured for HT:TBA-T3A and HT:TBA-T12A blockades corresponded to the capture frequency of HT:TBA in mode A (L1a blockades) and HT:TBA in mode B (L1b blockades), respectively.

Conflict of Interest: The authors declare no competing financial interest.

Supporting Information Available: Additional figures showing HT:TBA blockades to type I and II ClyA-CS nanopores and the values of the frequency of L1a and L1b blockades to type II ClyA-CS nanopores. This material is available free of charge *via* the Internet at http://pubs.acs.org.

Acknowledgment. We thank the European Research Council (European Commission's Seventh Framework Programme, project no. 260884) for funding. V.V.M. thanks the Research Foundation Flanders for the doctoral fellowship.

REFERENCES AND NOTES

1. Hurt, N.; Wang, H.; Akeson, M.; Lieberman, K. R. Specific Nucleotide Binding and Rebinding to Individual DNA Polymerase Complexes Captured on a Nanopore. *J. Am. Chem. Soc.* **2009**, 3772–3778.
2. Cockroft, S. L.; Chu, J.; Amorin, M.; Ghadiri, M. R. A Single-Molecule Nanopore Device Detects DNA Polymerase Activity with Single-Nucleotide Resolution. *J. Am. Chem. Soc.* **2008**, 818–820.
3. Bikwemu, R.; Wolfe, A. J.; Xing, X.; Movileanu, L. Facilitated Translocation of Polypeptides through a Single Nanopore. *J. Phys.: Condens. Matter* **2010**, 454117.
4. Wolfe, A. J.; Mohammad, M. M.; Cheley, S.; Bayley, H.; Movileanu, L. Catalyzing the Translocation of Polypeptides through Attractive Interactions. *J. Am. Chem. Soc.* **2007**, 14034–14041.
5. Movileanu, L.; Schmittschmitt, J. P.; Scholtz, J. M.; Bayley, H. Interactions of Peptides with a Protein Pore. *Biophys. J.* **2005**, 1030–1045.
6. Payet, L.; Martinho, M.; Pastoriza-Gallego, M.; Betton, J. M.; Auvray, L.; Pelta, J.; Mathe, J. Thermal Unfolding of Proteins Probed at the Single Molecule Level Using Nanopores. *Anal. Chem.* **2012**, 4071–4076.
7. Pastoriza-Gallego, M.; Rabah, L.; Gibrat, G.; Thiebot, B.; van der Goot, F. G.; Auvray, L.; Betton, J. M.; Pelta, J. Dynamics of Unfolded Protein Transport through an Aerolysin Pore. *J. Am. Chem. Soc.* **2011**, 2923–2931.
8. Oukhaled, G.; Mathé, J.; Biance, A.-L.; Bacri, L.; Betton, J.-M.; Lairez, D.; Pelta, J.; Auvray, L. Unfolding of Proteins and Long Transient Conformations Detected by Single Nanopore Recording. *Phys. Rev. Lett.* **2007**, 158101.
9. Stefureac, R.; Waldner, L.; Howard, P.; Lee, J. S. Nanopore Analysis of a Small 86-Residue Protein. *Small* **2008**, 59–63.
10. Stefureac, R.; Long, Y. T.; Kraatz, H. B.; Howard, P.; Lee, J. S. Transport of Alpha-Helical Peptides through Alpha-Hemolysin and Aerolysin Pores. *Biochemistry* **2006**, 9172–9179.
11. Rodriguez-Larrea, D.; Bayley, H. Multistep Protein Unfolding during Nanopore Translocation. *Nat. Nanotechnol.* **2013**, 288–295.
12. Nivala, J.; Marks, D. B.; Akeson, M. Unfoldase-Mediated Protein Translocation through an Alpha-Hemolysin Nanopore. *Nat. Biotechnol.* **2013**, 247–250.
13. Fologea, D.; Ledden, B.; McNabb, D. S.; Li, J. Electrical Characterization of Protein Molecules by a Solid-State Nanopore. *Appl. Phys. Lett.* **2007**, 539011–539013.
14. Han, A.; Creus, M.; Schurmann, G.; Linder, V.; Ward, T. R.; de Rooij, N. F.; Staufer, U. Label-Free Detection of Single Protein Molecules and Protein-Protein Interactions Using Synthetic Nanopores. *Anal. Chem.* **2008**, 4651–4658.
15. Stefureac, R. I.; Trivedi, D.; Marziali, A.; Lee, J. S. Evidence That Small Proteins Translocate through Silicon Nitride Pores in a Folded Conformation. *J. Phys.: Condens. Matter* **2010**, 454133.
16. Oukhaled, A.; Bacri, L.; Pastoriza-Gallego, M.; Betton, J. M.; Pelta, J. Sensing Proteins through Nanopores: Fundamental to Applications. *ACS Chem. Biol.* **2012**, 1935–1949.
17. Firnkes, M.; Pedone, D.; Knezevic, J.; Doblinger, M.; Rant, U. Electrically Facilitated Translocations of Proteins through Silicon Nitride Nanopores: Conjoint and Competitive Action of Diffusion, Electrophoresis, and Electroosmosis. *Nano Lett.* **2010**, 2162–2167.
18. Yusko, E. C.; Johnson, J. M.; Majd, S.; Prangkio, P.; Rollings, R. C.; Li, J.; Yang, J.; Mayer, M. Controlling Protein Translocation through Nanopores with Bio-Inspired Fluid Walls. *Nat. Nanotechnol.* **2011**, 253–260.
19. Japrung, D.; Dogan, J.; Freedman, K. J.; Nadzeyka, A.; Bauerdick, S.; Albrecht, T.; Kim, M. J.; Jemth, P.; Edel, J. B. Single-Molecule Studies of Intrinsically Disordered Proteins Using Solid-State Nanopores. *Anal. Chem.* **2013**, 2449–2456.
20. Wei, R.; Gatterdam, V.; Wieneke, R.; Tampe, R.; Rant, U. Stochastic Sensing of Proteins with Receptor-Modified Solid-State Nanopores. *Nat. Nanotechnol.* **2012**, 257–263.
21. Smeets, R. M.; Kowalczyk, S. W.; Hall, A. R.; Dekker, N. H.; Dekker, C. Translocation of Reca-Coated Double-Stranded DNA through Solid-State Nanopores. *Nano Lett.* **2009**, 3089–3096.
22. Mahmood, M. A.; Ali, W.; Adnan, A.; Iqbal, S. M. 3d Structural Integrity and Interactions of Single-Stranded Protein-Binding DNA in a Functionalized Nanopore. *J. Phys. Chem. B* **2014**, 5799–5806.
23. Japrung, D.; Bahrami, A.; Nadzeyka, A.; Peto, L.; Bauerdick, S.; Edel, J. B.; Albrecht, T. Ssb Binding to Single-Stranded DNA Probed Using Solid-State Nanopore Sensors. *J. Phys. Chem. B* **2014**, 11605–11612.
24. Raillon, C.; Cousin, P.; Traversi, F.; Garcia-Cordero, E.; Hernandez, N.; Radenovic, A. Nanopore Detection of Single Molecule RNAp-DNA Transcription Complex. *Nano Lett.* **2012**, 1157–1164.
25. Plesa, C.; Kowalczyk, S. W.; Zinsmeester, R.; Grosberg, A. Y.; Rabin, Y.; Dekker, C. Fast Translocation of Proteins through Solid State Nanopores. *Nano Lett.* **2013**, 658–663.
26. Soskine, M.; Biesemans, A.; De Maeyer, M.; Maglia, G. Tuning the Size and Properties of ClyA Nanopores Assisted by Directed Evolution. *J. Am. Chem. Soc.* **2013**, 13456–13463.
27. Soskine, M.; Biesemans, A.; Moeyaert, B.; Cheley, S.; Bayley, H.; Maglia, G. An Engineered ClyA Nanopore Detects Folded Target Proteins by Selective External Association and Pore Entry. *Nano Lett.* **2012**, 4895–4900.
28. Franceschini, L.; Soskine, M.; Biesemans, A.; Maglia, G. A Nanopore Machine Promotes the Vectorial Transport of DNA across Membranes. *Nat. Commun.* **2013**, 2415.
29. Mueller, M.; Grauschopf, U.; Maier, T.; Glockshuber, R.; Ban, N. The Structure of a Cytolytic Alpha-Helical Toxin Pore Reveals Its Assembly Mechanism. *Nature* **2009**, 726–730.
30. Biffi, G.; Tannahill, D.; McCafferty, J.; Balasubramanian, S. Quantitative Visualization of DNA G-Quadruplex Structures in Human Cells. *Nat. Chem.* **2013**, 182–186.
31. Wu, Y.; Brosh, R. M., Jr. G-Quadruplex Nucleic Acids and Human Disease. *FEBS J.* **2010**, 3470–3488.

32. Gonzalez, V.; Guo, K.; Hurley, L.; Sun, D. Identification and Characterization of Nucleolin as a C-Myc G-Quadruplex-Binding Protein. *J. Biol. Chem.* **2009**, 23622–23635.
33. Bidzinska, J.; Cimino-Reale, G.; Zaffaroni, N.; Folini, M. G-Quadruplex Structures in the Human Genome as Novel Therapeutic Targets. *Molecules* **2013**, 12368–12395.
34. Fry, M. Tetraplex DNA and Its Interacting Proteins. *Front. Biosci.* **2007**, 4336–4351.
35. von Hacht, A.; Seifert, O.; Menger, M.; Schutze, T.; Arora, A.; Konthur, Z.; Neubauer, P.; Wagner, A.; Weise, C.; Kurreck, J. Identification and Characterization of RNA Guanine-Quadruplex Binding Proteins. *Nucleic Acids Res.* **2014**, 6630–6644.
36. Pabo, C. O.; Nekludova, L. Geometric Analysis and Comparison of Protein-DNA Interfaces: Why Is There No Simple Code for Recognition? *J. Mol. Biol.* **2000**, 597–624.
37. Siggers, T. W.; Silkov, A.; Honig, B. Structural Alignment of Protein−DNA Interfaces: Insights into the Determinants of Binding Specificity. *J. Mol. Biol.* **2005**, 1027–1045.
38. Chen, F. E.; Ghosh, G. Regulation of DNA Binding by Rel/Nf-Kappab Transcription Factors: Structural Views. *Oncogene* **1999**, 6845–6852.
39. Burns, V.; Kerppola, T. K. Opposite Orientations of a Transcription Factor Heterodimer Bind DNA Cooperatively with Interaction Partners but Have Different Effects on Interferon-Beta Gene Transcription. *J. Biol. Chem.* **2012**, 31833–31844.
40. Chen, L.; Oakley, M. G.; Glover, J. N.; Jain, J.; Dervan, P. B.; Hogan, P. G.; Rao, A.; Verdine, G. L. Only One of the Two DNA-Bound Orientations of Ap-1 Found in Solution Cooperates with Nfatp. *Curr. Biol.* **1995**, 882–889.
41. Chytil, M.; Peterson, B. R.; Erlanson, D. A.; Verdine, G. L. The Orientation of the Ap-1 Heterodimer on DNA Strongly Affects Transcriptional Potency. *Proc. Natl. Acad. Sci. U.S.A.* **1998**, 14076–14081.
42. Bock, L. C.; Griffin, L. C.; Latham, J. A.; Vermaas, E. H.; Toole, J. J. Selection of Single-Stranded DNA Molecules That Bind and Inhibit Human Thrombin. *Nature* **1992**, 564–566.
43. Padmanabhan, K.; Tulinsky, A. An Ambiguous Structure of a DNA 15-Mer Thrombin Complex. *Acta Crystallogr. Sect. A: Found. Crystallogr.* **1996**, 272–282.
44. Russo Krauss, I.; Merlino, A.; Randazzo, A.; Novellino, E.; Mazzarella, L.; Sica, F. High-Resolution Structures of Two Complexes between Thrombin and Thrombin-Binding Aptamer Shed Light on the Role of Cations in the Aptamer Inhibitory Activity. *Nucleic Acids Res.* **2012**, 8119–8128.
45. Pica, A.; Russo Krauss, I.; Merlino, A.; Nagatoishi, S.; Sugimoto, N.; Sica, F. Dissecting the Contribution of Thrombin Exosite I in the Recognition of Thrombin Binding Aptamer. *FEBS J.* **2013**, 6581–6588.
46. Kawano, R.; Osaki, T.; Sasaki, H.; Takinoue, M.; Yoshizawa, S.; Takeuchi, S. Rapid Detection of a Cocaine-Binding Aptamer Using Biological Nanopores on a Chip. *J. Am. Chem. Soc.* **2011**, 8474–8477.
47. Wang, Y.; Zheng, D.; Tan, Q.; Wang, M. X.; Gu, L. Q. Nanopore-Based Detection of Circulating Micrornas in Lung Cancer Patients. *Nat. Nanotechnol.* **2011**, 668–674.
48. Mohammad, M. M.; Iyer, R.; Howard, K. R.; McPike, M. P.; Borer, P. N.; Movileanu, L. Engineering a Rigid Protein Tunnel for Biomolecular Detection. *J. Am. Chem. Soc.* **2012**, 9521–9531.
49. Arnaut, V.; Langecker, M.; Simmel, F. C. Nanopore Force Spectroscopy of Aptamer-Ligand Complexes. *Biophys. J.* **2013**, 1199–1207.
50. An, N.; Fleming, A. M.; Middleton, E. G.; Burrows, C. J. Single-Molecule Investigation of G-Quadruplex Folds of the Human Telomere Sequence in a Protein Nanocavity. *Proc. Natl. Acad. Sci. U.S.A.* **2014**, 14325–14331.
51. Rotem, D.; Jayasinghe, L.; Salichou, M.; Bayley, H. Protein Detection by Nanopores Equipped with Aptamers. *J. Am. Chem. Soc.* **2012**, 2781–2787.
52. Macaya, R. F.; Waldron, J. A.; Beutel, B. A.; Gao, H.; Joesten, M. E.; Yang, M.; Patel, R.; Bertelsen, A. H.; Cook, A. F. Structural and Functional Characterization of Potent Antithrombotic Oligonucleotides Possessing Both Quadruplex and Duplex Motifs. *Biochemistry* **1995**, 4478–4492.
53. German, I.; Buchanan, D. D.; Kennedy, R. T. Aptamers as Ligands in Affinity Probe Capillary Electrophoresis. *Anal. Chem.* **1998**, 4540–4545.
54. Gong, M.; Nikcevic, I.; Wehmeyer, K. R.; Limbach, P. A.; Heineman, W. R. Protein-Aptamer Binding Studies Using Microchip Affinity Capillary Electrophoresis. *Electrophoresis* **2008**, 1415–1422.
55. Huang, C.-C.; Cao, Z.; Chang, H.-T.; Tan, W. Protein−Protein Interaction Studies Based on Molecular Aptamers by Affinity Capillary Electrophoresis. *Anal. Chem.* **2004**, 6973–6981.
56. Berezovski, M.; Nutiu, R.; Li, Y.; Krylov, S. N. Affinity Analysis of a Protein−Aptamer Complex Using Nonequilibrium Capillary Electrophoresis of Equilibrium Mixtures. *Anal. Chem.* **2003**, 1382–1386.
57. Pinto, A.; Bermudo Redondo, M. C.; Ozalp, V. C.; O'Sullivan, C. K. Real-Time Apta-Pcr for 20 000-Fold Improvement in Detection Limit. *Mol. Biosyst.* **2009**, 548–553.
58. Ostatna, V.; Vaisocherova, H.; Homola, J.; Hianik, T. Effect of the Immobilisation of DNA Aptamers on the Detection of Thrombin by Means of Surface Plasmon Resonance. *Anal. Bioanal. Chem.* **2008**, 1861–1869.
59. Wilson, K. A.; Kellie, J. L.; Wetmore, S. D. DNA-Protein Pi-Interactions in Nature: Abundance, Structure, Composition and Strength of Contacts between Aromatic Amino Acids and DNA Nucleobases or Deoxyribose Sugar. *Nucleic Acids Res.* **2014**, 6726–6741.
60. Kunapuli, S. P.; Bradford, H. N.; Jameson, B. A.; DeLa Cadena, R. A.; Rick, L.; Wassell, R. P.; Colman, R. W. Thrombin-Induced Platelet Aggregation Is Inhibited by the Heptapeptide Leu271-Ala277 of Domain 3 in the Heavy Chain of High Molecular Weight Kininogen. *J. Biol. Chem.* **1996**, 11228–11235.
61. Maglia, G.; Heron, A. J.; Stoddart, D.; Japrung, D.; Bayley, H. Analysis of Single Nucleic Acid Molecules with Protein Nanopores. *Meth. Enzymol.* **2010**, 591–623.